Geophysical Research Letters

RESEARCH LETTER
10.1029/2020GL087002

Future Interactions Between Sea Level Rise, Tides, and Storm Surges in the World's Largest Urban Area

Michela De Dominicis[1], Judith Wolf[1], Svetlana Jevrejeva[1, 2], Peng Zheng[3,4], and Zhan Hu[5,6]

[1]National Oceanography Centre, Liverpool, UK, [2]Centre for Climate Research Singapore, Singapore, [3]School of Engineering, University of Liverpool, Liverpool, UK, [4]College of Oceanic and Atmospheric Sciences, Ocean University of China, Qingdao, China, [5]School of Marine Science, Sun Yat-sen University, Guangzhou, China, [6]Southern Marine Science and Engineering Guangdong Laboratory, Zhuhai, China

Abstract The Pearl River Delta contains the world's largest urban area in both size and population. It is a low-lying flood-prone coastal environment exposed to sea level rise (SLR) and extreme water levels caused by typhoons. A Finite Volume Community Ocean Model implementation for the South China Sea and the Pearl River Delta is used to understand how future SLR, tides, and typhoon storm surges will interact and affect coastal inundation. The SLR signal and extreme surge levels provide the major contributions to flooding; however, amplification of tides could exceed 0.5 m for 2.1 m SLR and should be considered when planning future coastal defences. On the other hand, if typhoons like Hato or Mangkhut, the latest and strongest ones hitting the area, were to happen in the future, a surge level reduction up to 0.5 m could be expected in coastal areas.

Key Points:
- In delta environments, sea level rise is not simply added to extreme water levels but induces feedbacks on tides and surge levels
- In the Pearl River Delta, amplification of tides exceeds 0.5 m for 2.1 m sea level rise, which is relevant for planning of coastal defences
- For a sea level rise of 2.1 m, a reduction of surge level of up to 0.5 m occurs in coastal areas for typhoons like Hato or Mangkhut

Supporting Information:
- Supporting Information S1

Correspondence to:
M. De Dominicis and Z. Hu
micdom@noc.ac.uk
huzh9@mail.sysu.edu.cn

Citation:
De Dominicis, M., Wolf, J., Jevrejeva, S., Zheng, P., & Hu, Z. (2020). Future interactions between sea level rise, tides, and storm surges in the world's largest urban area. *Geophysical Research Letters*, *47*, e2020GL087002. https://doi.org/10.1029/2020GL087002

Received 7 JAN 2020
Accepted 30 JAN 2020
Accepted article online 03 FEB 2020

1. Introduction

China's Pearl River Delta (PRD), located in the Guangdong province in the southern part of China, has experienced rapid population and economic growth since the 1980s. The PRD is an extensive river system that combines three major tributaries of the Pearl River: the North, East, and West rivers. As well as the delta itself, PRD refers to the urban agglomeration of nine cities (Guangzhou, Shenzhen, Zhuhai, Foshan, Dongguan, Zhongshan, Jiangmen, Huizhou, and Zhaoqing) and China's special administrative regions of Hong Kong and Macao (see Figure 1a for locations). With a growth rate of 4.5% per year, by 2010, the PRD megacity had surpassed Tokyo as the world's largest urban area in both size and population (World Bank et al., 2015)and the total number of inhabitants now exceeds 60 million. The PRD's GDP exceeds 1 trillion U.S. dollars, which would place it in the ranking of the top 20 national economies worldwide (Guangdong Statistical Bureau, 2017; International Monetary Fund, 2018).

The PRD is a low-lying coastal area, with much of its surface area less than 2 m above mean sea level (MSL) (Syvitski et al., 2009; Wu et al., 2018). It is exposed to current and future sea level rise (SLR) (He et al., 2014; Huang et al., 2004; Qu et al., 2018) and to extreme water levels generated by typhoons in the Western Pacific and South China Sea (Li et al., 2018; Yang et al., 2015). There are other delta megacities around the world facing similar challenges: for example, Kolkata and Dhaka (Ganges-Brahmaputra), Yangon (Irrawaddy), Bangkok (Chao Phraya), Ho Chi Minh City (Mekong), Shangai (Yangtze), Alexandria and Cairo (Nile) (Syvitski & Saito, 2007; Syvitski et al., 2009). Among those, Guangzhou, the largest city in the PRD, is the world's most economically vulnerable city to rising sea levels, with 16% of its population living within 0.5 m of present-day MSL. Estimated flood losses for Guangzhou exceed 13 billion U.S. dollars by 2050 in the scenario of a relative sea level increase of 0.6 m (including subsidence and SLR) and with adaptation to maintain present flood probability (Hallegatte et al., 2013). Shenzhen, the second largest city in the PRD, is also high in the ranking, being the ninth city in the world in terms of present estimated annual losses due to flooding, reaching the fourth place by 2050 (Hallegatte et al., 2013). Under the same 2050 scenario, Hong Kong is also among the top 50 cities in terms of future flood losses, although these are projected to be 100 times smaller than in Guangzhou (Hallegatte et al., 2013).

From the perspective of coastal flooding, there are various mechanisms, spanning a wide range of time scales, that together define extreme water level events: (1) the long-term annual-to-decadal scale of SLR, (2)

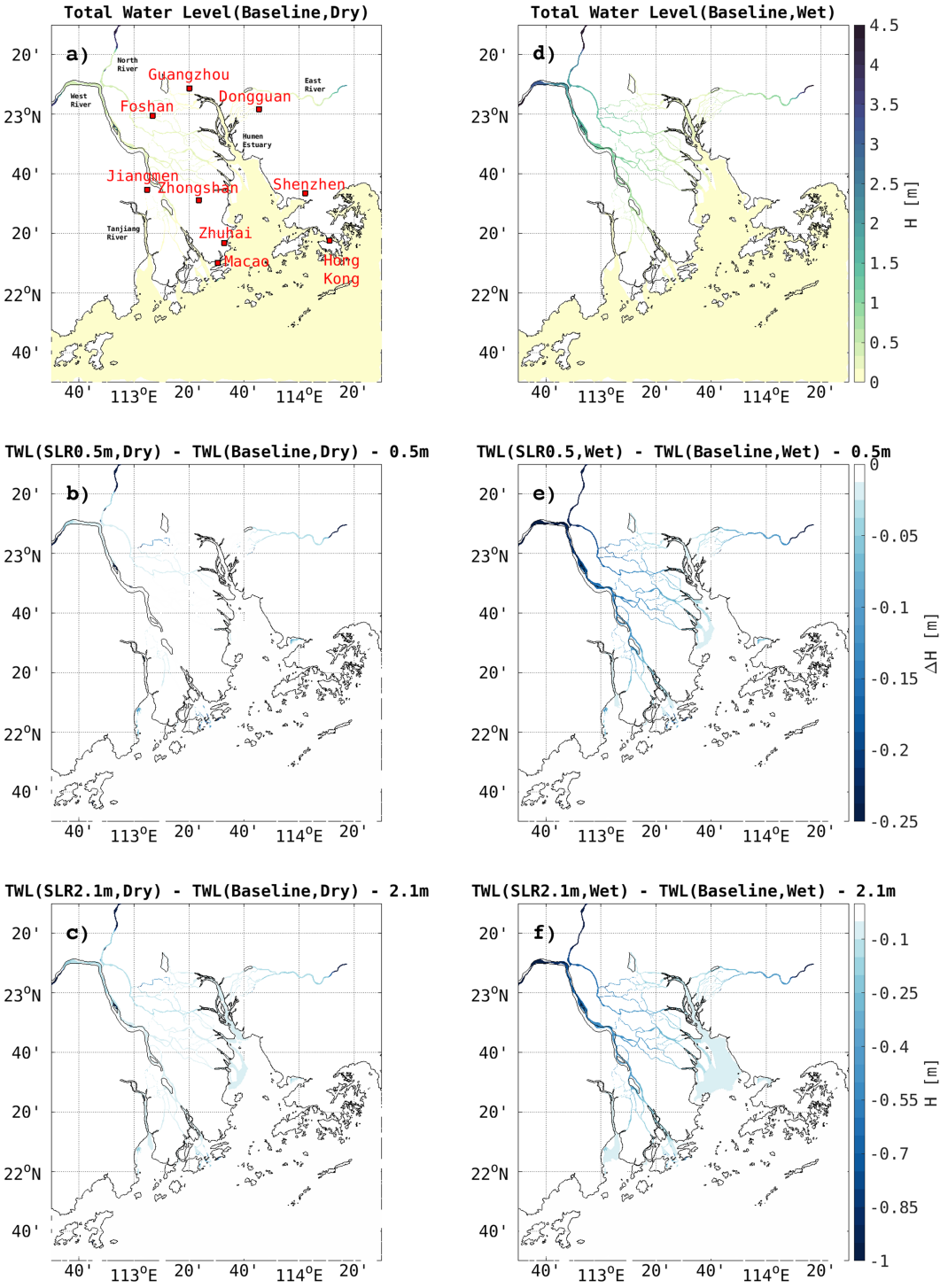

Figure 1. Total water level changes due to 0.5 and 2.1 m SLR: present average total water level during the dry season (a) and during the wet season (d); change in average total water level with 0.5 m SLR during the dry season (b) and during the wet season (e); change in average total water level with 2.1 m SLR during the dry season (c) and during the wet season (f). The future change in average total water level is calculated as the difference between the future minus the SLR imposed at the boundary and the present average future total water level.

the annual and interannual variability of freshwater discharges due to seasonal monsoon climate, (3) the daily scale of weather-related wave and surge events, and (4) the semidiurnal to diurnal scale of astronomical tidal oscillations. SLR increases the frequency of storm surge-induced flooding, because it sets a higher water level such that even low-to-moderate coastal surges become more likely to overtop existing coastal defences (Arns et al., 2017; Vitousek et al., 2017; Wang et al., 2017). Thus, even if typhoons do not get stronger or more frequent in the future (this is still much debated: Sobel et al., 2016; Stocker et al., 2013; Walsh et al., 2016), major increases in future flood risk will still be driven by SLR (Rahmstorf, 2017). The cumulative impact of more frequent flooding events due to SLR could be comparable to those events presently infrequent but more extreme (Moftakhari et al., 2017).

As intermittent flooding is mainly a consequence of extreme water levels, rather than MSL, it is essential to consider both regional trends in MSL and how those will interact with coastal processes. The presence of the coast and shallow waters results in processes, such as tides, being considerably more complex than offshore, which in turn result in a coastal modification of the larger-scale sea level variability (Woodworth et al., 2019). Thus, MSL, storm surge, and tides cannot just be added together when planning coastal protection measures as the size, depth, and width of estuaries and bays will strongly influence the tidal and storm surge dynamics, and their interactions with SLR (Bilskie et al., 2014; 2016; Du et al., 2018; Familkhalili & Talke, 2016; Holleman & Stacey, 2014; Idier et al., 2019; Passeri et al., 2015). This makes necessary a site-specific study to quantify the tide-surge-SLR interactions in the PRD. The questions to be answered in this paper are as follows: (i) What intensification in extreme water levels can we expect in the PRD under future climate conditions? (ii) What is the role played by SLR-tide-surge interactions in the coastal flooding patterns?

To answer those questions, we have built an FVCOM (Finite-Volume Community Ocean Model; Chen et al., 2003) implementation for the South China Sea and PRD. The model has an unstructured grid that extends from a coarse grid in the open ocean where tides and sea level changes are introduced, to an appropriate high resolution (100 m) in the delta distributary channels (see the supporting information for the description of the model setup and validation). In this study, we explore how the mean SLR signal coming from the open ocean interacts with coastal processes in the PRD, and whether tidal range and mean high water also increase with SLR. Additionally, we study how the surges generated by the two most recent and strongest typhoons that impacted the PRD, Typhoon Hato (2017) and Typhoon Mangkhhut (2018), would change under future sea level conditions.

2. Materials and Method

To explore the effect of SLR on the tidal dynamics, we chose to run the model for 1 month from the 15 December 1986 to the 15 January 1987 (the model was started 5 days earlier to allow for spin-up), including the highest astronomical tide that occurred on the 1 January 1987. The future MSL increase is imposed only along the model domain boundary, added to the tidal elevations (Egbert & Erofeeva, 2002, see the supporting information). This method allows the SLR to propagate through the domain guided by the models' governing equations (during spin-up), much like a tidal forcing without periodicity. With this dynamic approach the increase in sea level is deterministically established in the model domain, whereas a static approach would require to increase the baseline water levels everywhere in the model domain by the amount of SLR (Hagen & Bacopoulos, 2012), that is, by introducing a new bathymetry. The tidal forcing is kept the same for the present and future SLR scenarios.

In this work we model under four future SLR scenarios: 0.3, 0.5, 0.9, and 2.1 m. These correspond to the median (50th percentile) and upper limit (95th percentile) by 2050 (0.3 and 0.5 m, respectively) and by 2100 (0.9 and 2.1 m, respectively) of the regional sea level projections for the "High-end" RCP 8.5 future climate scenario, taken from Jackson and Jevrejeva (2016). The RCP8.5 scenario (Moss et al., 2010) is the "business as usual" (high greenhouse gases emissions) future climate scenario. "High-end" means that the SLR projections include an increased ice-sheet contribution using the expert elicitation of Bamber and Aspinall (2013), which leads to a global SLR higher than that of the Fifth Assessment Report of the Intergovernmental Panel on Climate Change (IPCC AR5) (Church et al., 2013). Moreover, we consider here regional sea level projections, as changes in future sea level will not occur uniformly around the globe. Indeed, the PRD local upper limit of 2.1 m is 30 cm higher than the global average by 2100 (1.8 m) (Jevrejeva et al., 2016). While the choice of the four future SLR scenarios has been based on these assumptions, the model experiments do not necessarily correspond to water levels for a particular MSL projection for a specific climate scenario or time

horizon. The applicability of our results is much broader, for example, 0.3 m is the RCP 8.5 scenario in 2040 (95th percentile) and 0.5 m could equally apply to the RCP 4.5 scenario in 2060 (95th percentile) or in 2090 (50th percentile), while 0.9 m is the upper limit in 2100 for the RCP 4.5 scenario (Jackson & Jevrejeva, 2016).

Since the PRD shows a significant seasonal river discharge variation, 10 model runs have been performed to explore the effects of SLR on tidal dynamics and how those are modulated by the seasonal river discharge (see Experiments 1–10 in Table S1 in the supporting information); each of the future SLR scenarios have been simulated for wet and dry seasonal conditions (Zhang et al., 2012).

To explore the effects of SLR on storm surge dynamics, we study the two most recent typhoons that impacted the PRD. Since 1950 there have been a total of 16 typhoons that necessitated the issuance of the Hurricane Signal No. 10 (the most severe warning) in Hong Kong. The latest have been Hato (2017) and Mangkhut (2018). They are among the strongest typhoons to affect the coastal areas of the PRD over the last several decades (Li et al., 2018). To reproduce these typhoon events, we forced the FVCOM PRD model with wind velocity and air pressure calculated using the Holland parametric model (Holland, 1980; Holland et al., 2010), which uses observed maximum wind speed and radius of maximum winds to calculate radial profiles of sea level pressure and winds in a tropical cyclone. Observations were obtained from 3-hourly data provided by the International Best Track Archive for Climate Stewardship (IBTrACS) Version 4. This approach was preferred to the usage of the ERA5 reanalysis, as we found that the peaks in wind velocity (and thus in water levels) were underestimated using the latter (see Figure S5).

For both typhoons we ran 15 different model experiments (see Table S1) to explore the effect of the four SLR scenarios. Since typhoons usually impact the PRD during the wet season, we do not consider the additional modulation of the freshwater river discharge. Experiments 11–15 (for Hato) and 26–30 (for Mangkhut) allow the study of tide, surge, and SLR interactions; in these experiments the model has been fully forced by atmospheric forcing, tides, and SLR. Experiments 16–20 (for Hato) and 31–35 (for Mangkhut) allow the study of tides and SLR interactions and are needed for the calculation of the surge; the model has been forced by tides and SLR only at the model boundary. The surge can be calculated as the difference between the fully forced run (Experiments 11–15 and 26–30) and the corresponding tide-only forced run (Experiments 16–20 and 31–35) for a given SLR. Experiments 21–25 (for Hato) and 35–40 (for Mangkhut) allow the study of the surge and SLR interactions only (no tides); for these experiments the model has been forced by atmospheric forcing and SLR at the model boundary.

3. Results

Our modeling show that SLR dynamically affect water levels in the PRD during different seasonal conditions (Figures 1a and 1d) where the difference between wet and dry season is mainly seen in the western part of the delta. The average water level is 1–3 m larger during the wet season in the West river (see Figure 1a for location). This is due to the latter contributing 77% of the total Pearl River discharge and showing the larger seasonal variation (Wu et al., 2016). Figures 1b and 1c and Figures 1e and 1f show the difference between the future and the present average total water level minus the mean SLR imposed at the model boundaries for 0.5 and 2.1 m SLR (see Figure S6 for 0.3 and 0.9 m SLR). A value of zero indicates that the average total water level increases by the same amount as in the open ocean, a positive value means it is higher than the externally imposed value, and a negative value means it is lower than the external value. During the dry season, with 0.5 m SLR, the average total water level increase is 0.5 m everywhere in the PRD (Figure 1b), while during the wet season, the influence of SLR is opposed by the larger river discharge in the western part of delta (Figure 1e), where the mean SLR signal is halved. Similar behavior is observed with 2.1 m SLR, the average total water level increases by 2.1 m everywhere in the delta during the dry season (Figure 1c), while the effect is halved by the river discharge during the wet season in the western river branches (Figure 1f). In this work we did not consider changes in the river discharge connected with future climate conditions.

We found that SLR can also intensify the severity of coastal flooding by introducing feedbacks on tides. The tide in the PRD has a mixed semidiurnal character, with a spring tidal range and a mean higher high water (MHHW) reaching 1.5 m; thus, it can be classified as a microtidal estuary (spring tidal range is defined as twice the sum of the M_2 and S_2 amplitudes, while MHHW is defined here as the sum of M_2, O_1, and K_1). The tide comes from the South China Sea and propagates from the east toward the PRD, where the tidal amplitude gradually increases. The maximum tidal range and amplitude occur in the upstream part of the Humen Estuary (see Figure 1a for location), where Guanzhou is located (see Figures 2a and 2d). A 0.5 m

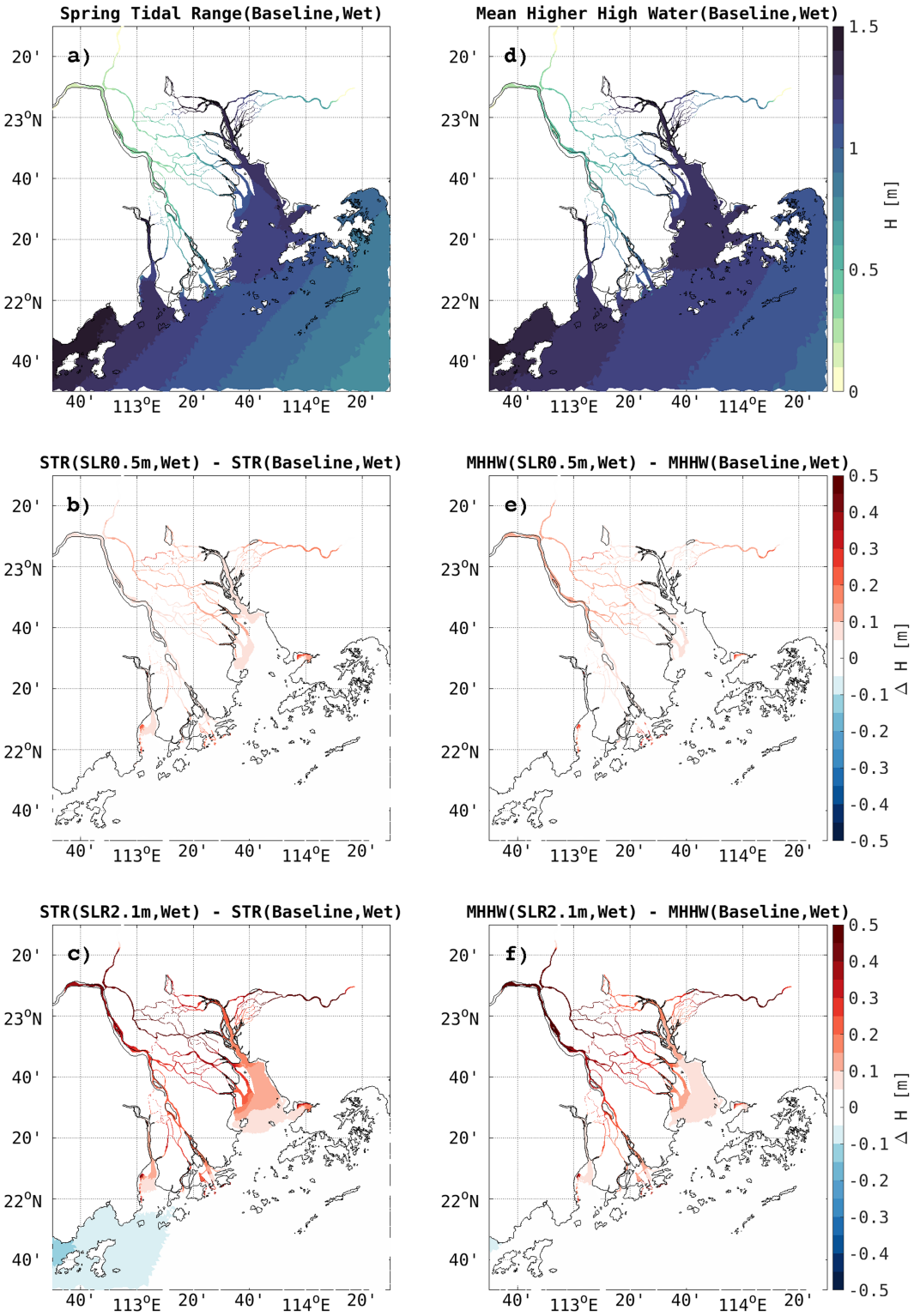

Figure 2. Tidal amplitude changes due to 0.5 and 2.1 m SLR (wet season): (a) present spring tidal range and predicted change with 0.5 m SLR (b) and with 2.1 m SLR (c); (d) present MHHW and predicted change with 0.5 m SLR (e) and with 2.1 m SLR (f).

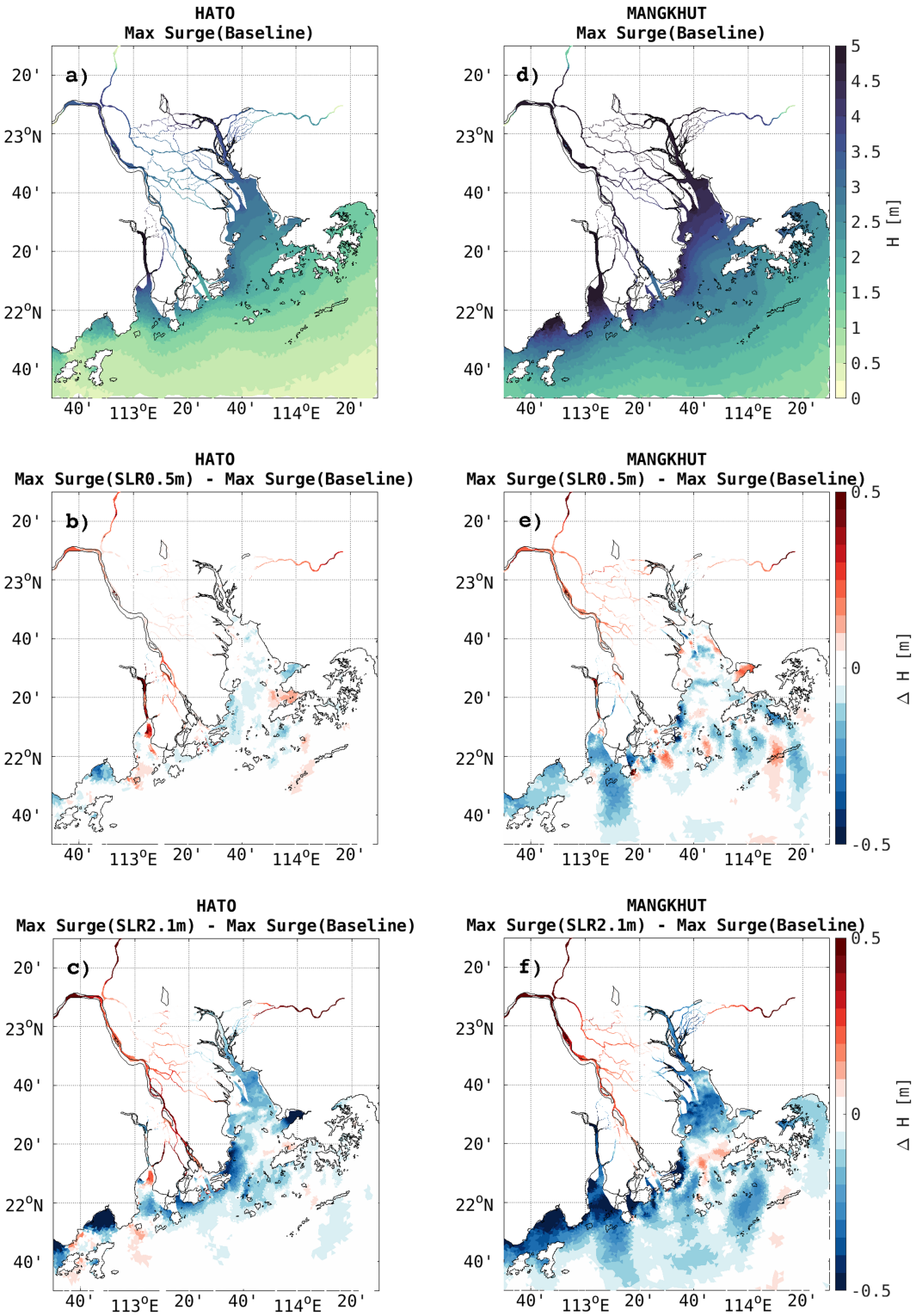

Figure 3. Storm surge changes due to 0.5 and 2.1 m SLR: present maximum surge level during typhoon Hato (a) and during typhoon Mangkhut (d); predicted change in the maximum surge level with 0.5 m SLR for Hato (b) and for Mangkhut (e); predicted change with 2.1 m SLR for Hato (c) and for Mangkhut (f).

SLR leads to an amplification of the tides in the upstream river branches of 5–15 cm, predicted for both the spring tidal range and the MHHW (see Figures 2b and 2e). With a SLR of 2.1 m, the amplification of the tides exceeds 0.5 m in the upper part of the West river (see Figures 2c and 2f). That river branch, under present conditions, shows a tidal range of about 0.5 m; thus, with 2.1 m SLR the tidal range will double, and the same occurs for the MHHW. Results shown in Figure 2 were obtained by including the wet season river discharge, as this can lead to more extreme changes. Indeed, we found that during the wet season, the larger average total water level, and thus less bottom friction, leads to a larger (by a few cm) increase in spring tidal range and MHHW in the central and western upper part of the delta (for the dry season results, see Figure S7). In the very upper part of the eastern river branches, however, the increase in spring tidal range and MHHW is larger during the dry season, as the river discharge is not suppressing the tidal dynamics there, as happens during the wet season. Changes in tidal range and MHHW with 0.3 and 0.9 m SLR are shown in the supporting information (Figures S8 and S9). With 0.3 m SLR, changes are visible only in the small river branches and are less then 10 cm. With 0.9 m SLR, changes follow the same pattern as for 0.5 and 2.1 m SLR, with intermediate values.

Lastly, we examined how SLR interacts with weather-related surge events (waves have not been considered in this work) through the change in water depth (surge heights depend upon this and coastal geometry). Our baseline model of storm surge generated by Typhoon Hato (Figure 3a) shows that the coastal cities of Macao and Zhuhai experienced a storm surge exceeding 2 m, which agrees with observations; the maximum storm surge recorded at the Zhuhai station was 2.79 m (Hong Kong Observatory, 2017). In Hong Kong the modeled storm surge is about 1 m (Figure 3a), reproducing local observations (Hong Kong Observatory, 2017). With a 0.5 m SLR (Figure 3b), the attenuation of the surge of less than 0.2 m is visible close to the Macao and Zhuhai coast, as well as on the opposite side of the river, where Shenzhen is located. With a 2.1 m SLR (Figure 3c), the attenuation of the surge is visible in the whole Humen estuary; it reaches 0.2–0.6 m at Macao, Zhuhai, and Shenzhen. In contrast, an increase of the surge is instead observed in the upper river branches with SLR (Figure 3c).

Mangkhut shows a greater wind intensity than Hato but happened on a neap tide rather than a spring tide. It induced a storm surge in Hong Kong of more than 2 m (Figure 3d), which agrees with observations (see Figure S5) and with the total water levels being the highest ever recorded (Hong Kong Observatory, 2018). Record-breaking storm surges were also recorded in many parts of the territory, with surges exceeding 4 m close to Zhuhai and Macao and in the whole Humen estuary (Figure 3d). The effect of SLR on the surge is similar to that observed for Hato, but with a stronger reduction of the surge. With 0.5 m SLR the reduction is slightly stronger and over a wider area than for Hato (Figure 3e), and with 2.1 m SLR the surge reduction reaches 0.5 m close to Macao and Zhuhai, and also along the coast close to the Tanjiang River (see Figure 1a for location), where the storm landed (Figure 3f). As found for Hato, an increase of the surge is instead observed in the river branches with both 0.5 m (Figure 3e) and 2.1 m SLR (Figure 3f). Changes in maximum surge levels with 0.3 and 0.9 m SLR are shown in the supporting information (Figure S10); they follow a similar pattern observed with 0.5 and 2.1 m SLR.

4. Discussion

Our results contribute to the developing literature on the role of SLR in coastal regions, and its impacts and interaction with tides (Carless et al., 2016; De Dominicis et al., 2018; Greenberg et al., 2012; Holleman & Stacey, 2014; Idier et al., 2017; Lee et al., 2017; Luz Clara et al., 2014; Passeri et al., 2015; 2016; Pelling, Uehara, et al., 2013; Pelling, Green, et al., 2013; Pelling & Green, 2013; Pickering et al., 2012; 2017; Ward et al., 2012). The changes in tides generated by SLR, shown in the previous section, are in line with previous studies for different semienclosed seas, shelf seas, and estuaries. Those studies showed that tidal amplitudes change due to SLR-induced depth changes and reduced bottom friction, and those changes are spatially variable. Focusing on the main PRD cities' locations (see Figure S14), the coastal cities of Hong Kong, Macao, and Zhuhai do not experience large changes in tidal amplitudes even with the largest 2.1 m SLR scenario. Moving upstream in the river branches, all cities show changes in tidal range/MHHW quasi-linearly increasing with SLR. Dongguan and Foshan experience the largest changes, with increases up to 0.5 m during the wet season in both tidal range and MHHW with 2.1 m SLR. Shenzhen is the only location showing a nonlinear behavior, with tidal changes reaching 0.4 m (for tidal range) and 0.3 m (for MHHW) with 0.9 m SLR, and not increasing further with 2.1 m SLR.

Storm surge can both amplify with SLR due to the decreased effect of bottom friction (Ali, 1999; Familkhalili & Talke, 2016; Liu & Huang, 2019) or diminish due to the reduction of the surface wind stress on the water column (Arns et al., 2015; 2017; Shen et al., 2019). Wind stress plays an important role in piling up water against the coast in shallow water, and the effect is inversely proportional to the water depth. This is why increasing MSL can lead to a reduction of the surface wind stress on the water column and thus to a decreased storm surge. In the PRD and for storms like Hato and Mangkhut, this effect has proven to be more relevant (especially for high SLR scenarios) than the reduced bottom friction, which would act in the opposite direction (increasing the surge). Indeed, Figure S11 shows that the difference between the wind stress and bottom stress terms (as written in the momentum equations, i.e., divided by density and total water depth and with the bottom stress with a negative sign) has positive values. This means that the wind stress is the dominant one. The combination of wind and bottom stress term decreases with increasing SLR in coastal areas, justifying the simultaneous decrease of the surge (as shown in Figures 3 and S10).

The increase in the maximum surge observed in the western river branches can be attributed to the interactions between tide, surge, and SLR. Indeed, Figures S12 and S13 show the change in surge with SLR, for both Hato and Mangkhut, generated only by the atmospheric forcing (no tides). With this setup, the atmospheric-only forced surge decreases everywhere; thus, it is only when the tides are also considered that the surge increases in the river branches (as shown in Figures 3 and S10). Additionally, SLR induces nonlinear changes in the maximum storm surge as shown in Figure S15 and in agreement with previous studies (Bilskie et al., 2016; Passeri et al., 2015). A nonlinear reduction in the maximum storm surge is observed for the coastal cities of Macao, Zhuhai, Hong Kong, and Shenzen for both typhoons for this range of SLR scenarios. Macao and Zhuhai experience the largest changes showing a 0.5–0.6 m decrease in the maximum storm surge during typhoon Mangkhut under 2.1 m SLR (Figure S15). With 2.1 m SLR, those cities located in the river branches show an increase in surge, not exceeding 20 cm, for typhoon Hato, while with the same SLR scenario, all the noncoastal cities, except for Foshan, experience a reduction in the maximum storm surge for typhoon Mangkhut (Figure S15).

Changes in tidal dynamics, of the same order of magnitude as the changes caused by SLR, have been already observed in the PRD. These changes are mainly caused by human activities, such as sand mining and land reclamation during the last 50 years to satisfy the needs of high population growth and urbanization (Cai et al., 2018; Zhang et al., 2015; 2009; 2010). These emerge as contemporary factors, which have not been considered in this work, and which will change the bottom topography of the delta, influencing tidal and surge propagation dynamics. We should consider that additional changes generated by SLR and SLR-tide-surge interactions have to be placed in the context of a fluvial basin already stressed by human activities and that can also be further augmented by natural and human-induced subsidence (Wang et al., 2012) and a change in river sediment fluxes due to river damming, irrigation, and mining (Wu et al., 2018).

An additional assumption of this study is that adaptation measures will be put in place and the PRD will be fully protected (i.e., no inundation is allowed beyond a fixed coastline) from SLR and the additional feedbacks on tides and surges we are presenting in this work. This is realistic given that the PRD is already protected by seawalls, although other studies (e.g., Lee et al., 2017; Pelling, Green, et al., 2013; Shen et al., 2019) have shown that allowing for inundation would lead to different results. Additionally, changes in the landscape (morphology, topography, sediment supply, and land use/land cover; e.g., Bilskie et al., 2014; Passeri et al., 2015; 2016; Siverd et al., 2019; Twilley et al., 2016; Yang et al., 2015) are not studied here but will be addressed in a continuation of this study.

5. Conclusions

The PRD is the largest urban agglomeration in the world but is located in a low-lying, deltaic, flood-prone coastal environment exposed to SLR as well as extreme water levels generated by seasonal river discharge-, tides-, and typhoons-induced surges. This study is the first to address SLR-tides-surge interactions in the PRD under several future mean water level scenarios. We used an FVCOM model implementation of the PRD region to explore the impact of projected SLR upon future tidal and storm surge water levels. We examined four future SLR scenarios: 0.3, 0.5, 0.9, and 2.1 m, which encompass the broad range of climate-scenario-based sea level projections making the results applicable across time horizons.

We found that the mean SLR from the open ocean will increase water levels in the PRD differently during the wet and the dry season. Cities on the western side of the delta will feel the effect of SLR less during the

wet season, because the effective SLR is halved by the river discharge, while cities in the eastern part of the delta will be more vulnerable.

We found that SLR can change the severity of coastal flooding by introducing feedbacks on tides and surge levels. In the PRD, tidal amplitudes change due to SLR-induced depth changes and consequent reduced bottom friction. A quasi-linear trend in tidal amplification with SLR has been observed for the main cities in the PRD. Amplification of spring tidal range and MHHW are about 0.1–0.5 m with SLR scenarios of 0.5–2.1 m, with cities located in the upstream river branches experiencing the largest changes (as Dongguan and Foshan reaching 0.5 m changes). Thus, the simple approach of just increasing the height of coastal defences by the amount of regional projected SLR might not be sufficient in some coastal regions since local changes in tidal amplitudes due to SLR have to be added on top of MSL changes, as already reported by Woodruff et al. (2013) and Arns et al. (2017).

Conversely, if typhoons such as Hato or Mangkhut were to happen in the future, a surge level reduction exceeding 0.5 m can be expected in some coastal areas for 2.1 m SLR, such as Macao and Zhuhai. In the PRD, the increased water depth due to SLR leads to the reduction of the surface wind stress on the water column, which has proven to be more important than the opposing effect of bottom friction. Thus, the surge reduction in coastal areas has the potential to counteract the increasing flood risk associated with SLR or changing tides. However, SLR feedbacks on surge are nonlinearly related to SLR and vary spatially. Indeed, an increase of the surge is observed in the river branches and it is associated with tide-surge-SLR interactions. Failure to account for these interactions can lead to a meaningful over/underestimation of local coastal exposure.

Acknowledgments
This work is part of the ANCODE (Applying nature-based coastal defence to the world's largest urban area—from science to practice) project, supported by a three-way international funding through the Netherlands Organisation for Scientific Research (NWO, lead funder, Grant ALWSD.2016.026), the China's National Natural Science Foundation (NSFC, Grant 51761135022), and the U.K. Research Councils (UKRI). The UK funding is through the NEWTON fund under the EPSRC Sustainable Deltas Programme, Grant EP/R024537/1. Typhoons best track data are from the IBTrACS (International Best Track Archive for Climate Stewardship) data set, provided by National Oceanic and Atmospheric Administration (NOAA) (https://www.ncdc.noaa.gov/ibtracs/). ERA5 reanalysis data were obtained from the European Centre for Medium Range Weather Forecasts (ECMWF) (https://www.ecmwf.int/en/forecasts/datasets/reanalysis-datasets/era5). For the model validation we used tide gauges data provided by the University of Hawaii Sea Level Center (https://uhslc.soest.hawaii.edu) and by Sun Yat-Sen University. The Pearl River Delta FVCOM model experiments presented in this manuscript are available online (at 10.5281/zenodo.3572509).

References

Ali, A. (1999). Climate change impacts and adaptation assessment in Bangladesh. *Climate Research*, *12*(2-3), 109–116.

Arns, A., Dangendorf, S., Jensen, J., Talke, S., Bender, J., & Pattiaratchi, C. (2017). Sea-level rise induced amplification of coastal protection design heights. *Scientific Reports*, *7*, 40171.

Arns, A., Wahl, T., Dangendorf, S., & Jensen, J. (2015). The impact of sea level rise on storm surge water levels in the northern part of the German Bight. *Coastal Engineering*, *96*, 118–131.

Bamber, J. L., & Aspinall, W. P. (2013). An expert judgement assessment of future sea level rise from the ice sheets. *Nature Climate Change*, *3*(4), 424.

Bilskie, M. V., Hagen, S. C., Alizad, K., Medeiros, S. C., Passeri, D. L., Needham, H. F., & Cox, A (2016). Dynamic simulation and numerical analysis of hurricane storm surge under sea level rise with geomorphologic changes along the northern Gulf of Mexico. *Earth's Future*, *4*(5), 177–193.

Bilskie, M. V., Hagen, S. C., Medeiros, S. C., & Passeri, D. L. (2014). Dynamics of sea level rise and coastal flooding on a changing landscape. *Geophysical Research Letters*, *41*, 927–934. https://doi.org/10.1002/2013GL058759

Cai, H., Huang, J., Niu, L., Ren, L., Liu, F., Ou, S., & Yang, Q. (2018). Decadal variability of tidal dynamics in the Pearl River Delta: Spatial patterns, causes, and implications for estuarine water management. *Hydrological Processes*, *32*(25), 3805–3819.

Carless, S. J., Green, J. A. M., Pelling, H. E., & Wilmes, S.-B. (2016). Effects of future sea-level rise on tidal processes on the Patagonian Shelf. *Journal of Marine Systems*, *163*, 113–124.

Chen, C., Liu, H., & Beardsley, R. C. (2003). An unstructured grid, finite-volume, three-dimensional, primitive equations ocean model: Application to coastal ocean and estuaries. *Journal of Atmospheric and Oceanic Technology*, *20*(1), 159–186.

Church, J. A., Clark, P. U., Cazenave, A., Gregory, J. M., Jevrejeva, S., Levermann, A., et al. (2013). Sea level change. Climate Change 2013: The Physical Science Basis, *Contribution of Working Group I to the Fifth Assessment Report of the Intergovernmental Panel on Climate Change* pp. 1137–1216). Cambridge, United Kingdom and New York, NY, USA: Cambridge University Press.

De Dominicis, M., Wolf, J., & O'Hara Murray, R. (2018). Comparative effects of climate change and tidal stream energy extraction in a shelf sea. *Journal of Geophysical Research: Oceans*, *123*, 5041–5067. https://doi.org/10.1029/2018JC013832

Du, J., Shen, J., Zhang, Y. J., Ye, F., Liu, Z., Wang, Z., et al. (2018). Tidal response to sea-level rise in different types of estuaries: The importance of length, bathymetry, and geometry. *Geophysical Research Letters*, *45*, 227–235. https://doi.org/10.1002/2017GL075963

Egbert, G. D., & Erofeeva, S. Y. (2002). Efficient inverse modeling of barotropic ocean tides. *Journal of Atmospheric and Oceanic Technology*, *19*(2), 183–204.

Familkhalili, R., & Talke, S. A. (2016). The effect of channel deepening on tides and storm surge: A case study of Wilmington, NC. *Geophysical Research Letters*, *43*, 9138–9147. https://doi.org/10.1002/2016GL069494

Greenberg, D. A., Blanchard, W., Smith, B., & Barrow, E. (2012). Climate change, mean sea level and high tides in the Bay of Fundy. *Atmosphere-ocean*, *50*(3), 261–276.

Guangdong Statistical Bureau (2017). *Guangdong Statistical Yearbook*: China Statistical Press.

Hagen, S. C., & Bacopoulos, P. (2012). Coastal flooding in Florida's Big Bend Region with application to sea level rise based on synthetic storms analysis. *Terrestrial Atmospheric and Oceanic Sciences*, *23*(5), 481.

Hallegatte, S., Green, C., Nicholls, R. J., & Corfee-Morlot, J. (2013). Future flood losses in major coastal cities. *Nature Climate Change*, *3*(9), 802.

He, L., Li, G., Li, K., & Shu, Y. (2014). Estimation of regional sea level change in the Pearl River Delta from tide gauge and satellite altimetry data. *Estuarine, Coastal and Shelf Science*, *141*, 69–77.

Holland, G. J. (1980). An analytic model of the wind and pressure profiles in hurricanes. *Monthly Weather Review*, *108*(8), 1212–1218.

Holland, G. J., Belanger, J. I., & Fritz, A. (2010). A revised model for radial profiles of hurricane winds. *Monthly Weather Review*, *12*, 4393–4401.

Holleman, R. C., & Stacey, M. T. (2014). Coupling of sea level rise, tidal amplification, and inundation. *Journal of Physical Oceanography*, *44*(5), 1439–1455.

Hong Kong Observatory (2017). Super Typhoon Hato (1713) 20 to 24 August 2017 report. https://www.weather.gov.hk/informtc/hato17/report.htm, last time accessed August 2019.

Hong Kong Observatory (2018). Super Typhoon Mangkhut (1822) 7 to 17 September 2018 report. https://www.weather.gov.hk/informtc/mangkhut18/report.htm, last time accessed August 2019.

Huang, Z., Zong, Y., & Zhang, W. (2004). Coastal inundation due to sea level rise in the Pearl River Delta, China. *Natural Hazards*, *33*(2), 247–264.

Idier, D., Bertin, X., Thompson, P., & Pickering, M. D. (2019). Interactions between mean sea level, tide, surge, waves and flooding: Mechanisms and contributions to sea level variations at the coast. *Surveys in Geophysics*, *40*(6), 1603–1630.

Idier, D., Paris, F., Le Cozannet, G., Boulahya, F., & Dumas, F. (2017). Sea-level rise impacts on the tides of the European Shelf. *Continental Shelf Research*, *137*, 56–71.

International Monetary Fund (2018). World Economic Outlook Database.

Jackson, L. P., & Jevrejeva, S. (2016). A probabilistic approach to 21st century regional sea-level projections using RCP and high-end scenarios. *Global and Planetary Change*, *146*, 179–189.

Jevrejeva, S., Jackson, L. P., Riva, R. E. M., Grinsted, A., & Moore, J. C. (2016). Coastal sea level rise with warming above 2 C. *Proceedings of the National Academy of Sciences*, *113*(47), 13,342–13,347.

Lee, S. B., Li, M., & Zhang, F. (2017). Impact of sea level rise on tidal range in Chesapeake and Delaware Bays. *Journal of Geophysical Research: Oceans*, *122*, 3917–3938. https://doi.org/10.1002/2016JC012597

Li, L., Yang, J., Lin, C.-Y., Chua, C. T., Wang, Y., Zhao, K., et al. (2018). Field survey of Typhoon Hato (2017) and a comparison with storm surge modeling in Macau. *Natural Hazards and Earth System Sciences*, *18*(12), 3167–3178.

Liu, W.-C., & Huang, W.-C. (2019). Influences of sea level rise on tides and storm surges around the Taiwan coast. *Continental Shelf Research*, *173*, 56–72.

Luz Clara, M., Simionato, C. G., D'Onofrio, E., & Moreira, D. (2014). Future sea level rise and changes on tides in the Patagonian continental shelf. *Journal of Coastal Research*, *31*(3), 519–535.

Moftakhari, H. R, AghaKouchak, A., Sanders, B. F., & Matthew, R. A. (2017). Cumulative hazard: The case of nuisance flooding. *Earth's Future*, *5*(2), 214–223.

Moss, R. H., Edmonds, J. A., Hibbard, K. A., Manning, M. R., Rose, S. K., Van V., et al. (2010). The next generation of scenarios for climate change research and assessment. *Nature*, *463*(7282), 747.

Passeri, D. L., Hagen, S. C., Medeiros, S. C., & Bilskie, M. V. (2015). Impacts of historic morphology and sea level rise on tidal hydrodynamics in a microtidal estuary (Grand Bay, Mississippi). *Continental Shelf Research*, *111*, 150–158.

Passeri, D. L., Hagen, S. C., Medeiros, S. C., Bilskie, M. V., Alizad, K., & Wang, D. (2015). The dynamic effects of sea level rise on low-gradient coastal landscapes: A review. *Earth's Future*, *3*(6), 159–181.

Passeri, D. L., Hagen, S. C., Plant, N. G., Bilskie, M. V., Medeiros, S. C., & Alizad, K. (2016). Tidal hydrodynamics under future sea level rise and coastal morphology in the Northern Gulf of Mexico. *Earth's Future*, *4*(5), 159–176.

Pelling, H. E., & Green, J. A. M. (2013). Sea level rise and tidal power plants in the Gulf of Maine. *Journal of Geophysical Research: Oceans*, *118*, 2863–2873. https://doi.org/10.1002/jgrc.20221

Pelling, H. E., Green, J. A. M., & Ward, S. L. (2013). Modelling tides and sea-level rise: To flood or not to flood. *Ocean Modelling*, *63*, 21–29.

Pelling, H. E., Uehara, K., & Green, J. A. M. (2013). The impact of rapid coastline changes and sea level rise on the tides in the Bohai Sea, China. *Journal of Geophysical Research: Oceans*, *118*, 3462–3472. https://doi.org/10.1002/jgrc.20258

Pickering, M. D., Horsburgh, K. J., Blundell, J. R., Hirschi, J. J.-M., Nicholls, R. J., Verlaan, M., & Wells, N. C. (2017). The impact of future sea-level rise on the global tides. *Continental Shelf Research*, *142*, 50–68.

Pickering, M. D., Wells, N. C., Horsburgh, K. J., & Green, J. A. M. (2012). The impact of future sea-level rise on the European Shelf tides. *Continental Shelf Research*, *35*, 1–15.

Qu, Y., Jevrejeva, S., Jackson, L. P., & Moore, J. C. (2018). Coastal sea level rise around the China Seas. *Global and Planetary Change*, *172*, 454–463.

Rahmstorf, S. (2017). Rising hazard of storm-surge flooding. *Proceedings of the National Academy of Sciences*, *114*(45), 11,806–11,808.

Shen, Y., Deng, G., Xu, Z., & Tang, J. (2019). Effects of sea level rise on storm surge and waves within the Yangtze River Estuary. *Frontiers of Earth Science*, *13*(2), 303–316.

Siverd, C. G., Hagen, S. C., Bilskie, M. V., Braud, D. H., Gao, S., Peele, R. H., & Twilley, R. R. (2019). Assessment of the temporal evolution of storm surge across coastal Louisiana. *Coastal Engineering*, *150*, 59–78.

Sobel, A. H., Camargo, S. J., Hall, T. M., Lee, C.-Y., Tippett, M. K., & Wing, A. A. (2016). Human influence on tropical cyclone intensity. *Science*, *353*(6296), 242–246.

Stocker, T. F., Qin, D., Plattner, G.-K., Tignor, M., Allen, S. K., Boschung, J., et al. (2013). Climate Change 2013: The physical science basis, *Contribution of Working Group I to the Fifth Assessment Report of the Intergovernmental Panel on Climate Change*. Cambridge, United Kingdom and New York, NY, USA: Cambridge University Press.

Syvitski, J. P. M., Kettner, A. J., Overeem, I., Hutton, E. W. H., Hannon, M. T., Brakenridge, G. R., et al. (2009). Sinking deltas due to human activities. *Nature Geoscience*, *2*(10), 681.

Syvitski, J. P. M., & Saito, Y. (2007). Morphodynamics of deltas under the influence of humans. *Global and Planetary Change*, *57*(3-4), 261–282.

Twilley, R. R., Bentley, S. J., Chen, Q., Edmonds, D. A., Hagen, S. C., Lam, N. S.-N., et al. (2016). Co-evolution of wetland landscapes, flooding, and human settlement in the Mississippi River Delta Plain. *Sustainability Science*, *11*(4), 711–731.

Vitousek, S., Barnard, P. L., Fletcher, C. H., Frazer, N., Erikson, L., & Storlazzi, C. D. (2017). Doubling of coastal flooding frequency within decades due to sea-level rise. *Scientific Reports*, *7*(1), 1399.

Walsh, K. J. E., McBride, J. L., Klotzbach, P. J., Balachandran, S., Camargo, S. J., Holland, G., et al. (2016). Tropical cyclones and climate change. *Wiley Interdisciplinary Reviews: Climate Change*, *7*(1), 65–89.

Wang, R.-Q., Herdman, L. M., Erikson, L., Barnard, P., Hummel, M., & Stacey, M. T. (2017). Interactions of estuarine shoreline infrastructure with multiscale sea level variability. *Journal of Geophysical Research: Oceans*, *122*, 9962–9979. https://doi.org/10.1002/2017JC012730

Wang, H., Wright, T. J., Yu, Y., Lin, H., Jiang, L., Li, C., & Qiu, G. (2012). InSAR reveals coastal subsidence in the Pearl River Delta, China. *Geophysical Journal International*, *191*(3), 1119–1128.

Ward, S. L., Green, J. A. M., & Pelling, H. E. (2012). Tides, sea-level rise and tidal power extraction on the European shelf. *Ocean Dynamics*, *62*(8), 1153–1167.

Woodruff, J. D., Irish, J. L., & Camargo, S. J. (2013). Coastal flooding by tropical cyclones and sea-level rise. *Nature*, *504*(7478), 44.

Woodworth, P. L., Melet, A., Marcos, M., Ray, R. D., Wöppelmann, G., Sasaki, Y. N., et al. (2019). Forcing factors affecting sea level changes at the coast. *Surveys in Geophysics*, *40*(6), 1351–1397.

World Bank (2015). *East Asia's Changing Urban Landscape: Measuring a Decade of Spatial Growth*, Urban Development Series. Washington, DC: World Bank. https://doi.org/10.1596/978-1-4648-0363-5

Wu, Z., Milliman, J. D., Zhao, D., Cao, Z., Zhou, J., & Zhou, C. (2018). Geomorphologic changes in the lower Pearl River Delta, 1850–2015, largely due to human activity. *Geomorphology*, *314*, 42–54.

Wu, C. S., Yang, S., Huang, S., & Mu, J. (2016). Delta changes in the Pearl River estuary and its response to human activities (1954–2008). *Quaternary International*, *392*, 147–154.

Yang, L., Scheffran, J., Qin, H., & You, Q. (2015). Climate-related flood risks and urban responses in the Pearl River Delta, China. *Regional Environmental Change*, *15*(2), 379–391.

Yang, Z., Wang, T., Voisin, N., & Copping, A. (2015). Estuarine response to river flow and sea-level rise under future climate change and human development. *Estuarine, Coastal and Shelf Science*, *156*, 19–30.

Zhang, W., Mu, S.-S., Zhang, Y.-J., & Chen, K.-M. (2012). Seasonal and interannual variations of flow discharge from Pearl River into sea. *Water Science and Engineering*, *5*(4), 399–409.

Zhang, W., Ruan, X., Zheng, J., Zhu, Y., & Wu, H. (2010). Long-term change in tidal dynamics and its cause in the Pearl River Delta, China. *Geomorphology*, *120*(3-4), 209–223.

Zhang, W., Xu, Y., Hoitink, A. J. F., Sassi, M. G., Zheng, J., Chen, X., & Zhang, C. (2015). Morphological change in the Pearl River Delta, China. *Marine Geology*, *363*, 202–219.

Zhang, W., Yan, Y., Zheng, J., Li, L., Dong, X., & Cai, H. (2009). Temporal and spatial variability of annual extreme water level in the Pearl River Delta region, China. *Global and Planetary Change*, *69*(1-2), 35–47.